PAPER • OPEN ACCESS

Vascular adaptation model from force balance: *Physarum polycephalum* as a case study

IOP Publishing New J. Phys. 25 (2023) 123052 https://doi.org/10.1088/1367-2630/ad1488

New Journal of Physics
The open access journal at the forefront of physics

Deutsche Physikalische Gesellschaft DPG
IOP Institute of Physics

Published in partnership with: Deutsche Physikalische Gesellschaft and the Institute of Physics

OPEN ACCESS

RECEIVED
2 March 2023

REVISED
28 November 2023

ACCEPTED FOR PUBLICATION
11 December 2023

PUBLISHED
29 December 2023

PAPER

Vascular adaptation model from force balance: *Physarum polycephalum* as a case study

Sophie Marbach[1,2], **Noah Ziethen**[3] and **Karen Alim**[3,4,*]

[1] CNRS, Sorbonne Université, Physicochimie des Electrolytes et Nanosystèmes Interfaciaux, F-75005 Paris, France
[2] Courant Institute of Mathematical Sciences, New York University, 251 Mercer Street, New York, NY 10012, United States of America
[3] Max Planck Institute for Dynamics and Self-Organization, Am Fassberg 17, 37077 Göttingen, Germany
[4] TUM School of Natural Sciences, Department of Bioscience, Center for Protein Assemblies (CPA), Technical University of Munich, Garching, Germany
[*] Author to whom any correspondence should be addressed.

E-mail: k.alim@tum.de

Keywords: vein adaptation, force balance, shear, Murray's law, vascular networks

Abstract

Understanding vascular adaptation, namely what drives veins to shrink or grow, is key for the self-organization of flow networks and their optimization. From the top–down principle of minimizing flow dissipation at a fixed metabolic cost within flow networks, flow shear rate resulting from the flows pervading veins is hypothesized to drive vein adaptation. Yet, there is no proposed mechanism of how flow forces impact vein dynamics. From the physical principle of force balance, shear rate acts parallel to vein walls, and hence, naively shear rate could only stretch veins and not dilate or shrink them. We, here, resolve this paradox by theoretically investigating force balance on a vein wall in the context of the vascular network of the model organism *Physarum polycephalum*. We propose, based on previous mechanical studies of cross-linked gels, that shear induces a nonlinear, orthogonal response of the actomyosin gel making up vein walls, that can indeed drive vein dilatation. Furthermore, our force balance approach allows us to identify that shear feedback occurs with a typical timescale and with a typical target shear rate that are not universal properties of the material but instead depend smoothly on the vein's location within the network. In particular, the target shear rate is related to the vein's hydrostatic pressure, which highlights the role of pressure in vascular adaptation in this context. Finally, since our derivation is based on force balance and fluid mechanics, we believe our approach can be extended, giving attention to specific differences, to describe vascular adaptation in other organisms.

1. Introduction

Vascular flow networks continuously reorganize by growing new veins or shrinking old ones [1–3], to optimize specific functions such as nutrient or information distribution or to adapt to changing environmental cues. As an example, we show in figure 1 the spontaneous reorganization of the slime mold *Physarum polycephalum* (*P. polycephalum*) over the course of a few hours, which shows significant vein trimming. Vascular adaptation is seen across the plant and animal realms: from blood vasculature [2, 4–6], via leaf venation in plants [7, 8] to vein networks making up fungi and slime molds [9, 10]. Understanding vascular adaptation is crucial to probe healthy development [2] and disease growth [11, 12].

At steady state, Murray's law [14] provides a rather reliable prediction of network morphologies across a variety of animals and plants [15–19]. Briefly, we recapitulate the main phenomenological ingredients yielding this law, based on the principle of minimum work. Murray stipulated [14] that energy dissipation in a vein of radius a and length L is given by shear dissipation and metabolic expense to sustain the vein

$$\mathcal{E} = \frac{1}{2}\frac{Q^2}{R} + \pi bLa^2 = \frac{4\mu LQ^2}{\pi a^4} + \pi bLa^2, \tag{1}$$

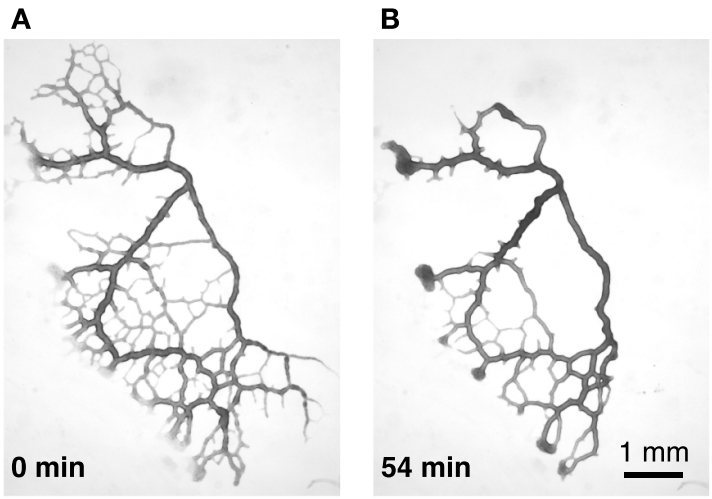

Figure 1. Bright-field images of a reorganizing specimen of *Physarum polycephalum*, from a reference state (A) and 54 min later (B). Adapted with permission from [13].

where $R = \pi a^4/8\mu L$ is the vein's hydraulic resistance assuming Poiseuille flow in the vein, b is a local metabolic constant per unit volume, Q the flow rate, and μ the fluid's viscosity. The principle of minimum energy expense suggests searching for the minimum of $\mathcal{E}$ with respect to the vein radius a, which gives the relation $a^6 = 8Q^2\mu/b\pi^2$. Here, and in what follows, we use the convention that for coordinates x_i and x_j, and fluid velocity components v_i and v_j, the shear rate components are $\tau_{ij} = \partial v_i/\partial x_j + \partial v_j/\partial x_i$. At a vessel wall undergoing Poiseuille flow, shear rate is usually defined as $\tau \equiv \tau_{rz}$ where r is the radial coordinate, and z the coordinate along the vessel wall. If we calculate the shear rate $\tau = 4Q/\pi a^3$ in this optimal state, we obtain that shear rate is constant and equal to an optimal value $\tau = \sqrt{b/\mu} \equiv \tau_0$, independent of vein radius *aa*.

Beyond the steady state, dynamic adaptation of veins has often been modeled relying on the following *phenomenological* adaptation equation for individual veins:

$$\frac{1}{a}\frac{da}{dt} = \frac{1}{t_{\text{adapt}}}\left(f(\tau) - f(\tau_0)\right) \tag{2}$$

where $a(t)$ is the vein radius at time t, t_{adapt} an adaptation timescale, $\tau$the local shear rate in the vein and $f(\tau)$ is a non-dimensional monotonically increasing function such that $f(\tau = 0) = 0$ [20]. We will specify the specific functional form $f(\tau)$ later. Note that we will, here, use τ to represent the shear *rate* in a vein. It is also common to discuss shear *stress* σ, which is related to the shear rate as $\sigma = \mu\tau$ where μ is again the fluid's viscosity. At steady state, the shear rate is constant and equal to the target shear rate value $\tau = \tau_0$, consistent with Murray's law. The parameters t_{adapt} and τ_0 are usually taken to be network dependent but constant across the organism [3, 8, 18, 20–29].

The variety of functions $f(\tau)$ used in such *phenomenological* models already points to a lack of consensus. Some works investigate $f(\tau) \sim |\tau|$ [18, 20–24, 28, 29] with possible generalizations and extensions [8], while others consider $f(\tau) \sim \log(\tau)$ [25, 26] and extensions [27]. Notably, a rather recent work [3] follows Murray's law of minimizing energy dissipation to arrive at $f(\tau) \sim \tau^2$. However, there is currently no effort to understand the mechanistic origin of such an adaptation rule. We, therefore, lack the chance to validate the functional dependence on shear rate.

In addition, an adaptation rule with shear rate driving tube dilation or shrinkage is rather counter-intuitive from a mechanical perspective. In all vascular biological networks [3, 8, 18, 20–27], the same laws govern laminar flow through slender veins: the shear rate τ, evaluated on the surface of a vein, acts on the longitudinal direction along the vein. Therefore, naively shear rate can only *extend a vein longitudinally*, but dilatation or shrinking, namely changes in the vein radius $a(t)$, may not arise. Other effects, such as the Bernoulli effect, highlight the role of pressure in vascular adaptation, which is discarded in shear oriented models as in equation (2). While the Bernoulli effect does not prevail in vasculature systems that often operate at low Reynolds numbers, the role of pressure needs to be better understood.

In this work, we reconcile the paradox of how shear rate can drive vein radius changes and derive equation (2) by establishing a detailed mechanical force balance on a vein wall. To this end, we focus our derivation on the broadly studied model organism *P. polycephalum*. One important specificity of *P. polycephalum* is that its veins are encapsulated in an actomyosin fiber cortex. For the latter, recent

experimental studies [30, 31] show that cross-linked actin fibers respond orthogonally to shear. We propose as a potential mechanism that such orthogonal response to shear may dilate or shrink veins beyond just acting in the longitudinal direction. The detailed characteristics of the actomyosin fiber cortex determine the exact shape of $f(\tau)$, which should be increasing with τ and for *P. polycephalum* is well approached by $f(\tau) \propto \tau^2$. Our investigation also shows that $f(\tau)$ could take other shapes according to the cortex's mechanical properties that vary across biological systems. Finally, and in contrast with previous assumptions, we find that t_{adapt} and τ_0 are *local* quantities that vary smoothly and slowly throughout the network but are location-specific. Interestingly, we find that τ_0 is related to local hydrostatic pressure, confirming the role of pressure in vascular adaptation. Our work, therefore, opens up the possibility of understanding vascular reorganization from experimental data; see our accompanying mostly experimental work [13].

2. Problem setup

We perform a force-balance derivation in the context of vascular adaptation of the veins formed by the prototypical slime mold *P. polycephalum*. While we make along the way several assumptions, we, here, discuss their validity in *P. polycephalum* and also their relevance in other systems. We recapitulate these approximations in table 1. We use these approximations for simplicity, assuming that fundamental aspects of the force transmissions are still conserved even in the light of these simplifying assumptions. In addition, these approximations allow us to identify essential modeling ingredients to exhibit an adaptation rule similar to equation (2).

2.1. *P. polycephalum*'s vasculature: model with a viscoelastic shell encapsulating a Newtonian fluid

Here, we investigate the vascular networks formed by the unicellular slime mold *P. polycephalum*. The body of the organism comprises a network of soft slender tubes. The tube walls enclose a cytoplasmic fluid that contains the nuclei and flows freely through the network [32]. An actin-rich actomyosin cortex is anchored to the cell membrane lining the tubes. Flows in the veins arise from rhythmic contractions of vein walls due to actomyosin activity in the cortex [33]. The period of oscillating flows and periodic contractions is rather fast, on the order of 1–2 min [34, 35], while long-term vein adaptation arises over 10–100 min. The gel-like walls of the tube are quite complex, forming a porous structure allowing fluid flow through small channels and invaginations along the wall [32].

While the structure of the tubes is complex, it has been shown that flows in *P. polycephalum* follow Poiseuille law rather remarkably [13, 36–38]. This means that cytoplasmic fluid can be treated as a Newtonian fluid. Flows nearly vanish at the inner wall boundaries, suggesting that the remaining flows inside the porous wall can be neglected as a first approximation. In addition, the wall's structure is gel-like, with a viscoelastic response [39, 40]. We will therefore treat the wall as a viscoelastic solid. Note that, assuming Newtonian fluid flow inside a viscoelastic shell is a common modeling framework in vasculature studies, in blood flow [41–44], in *P. polycephalum* [45], in leaf venation [46] and artificial systems [47].

2.2. Low Reynolds number flows in the contractile network

We model flow in a single vein filled with cytoplasmic fluid considered incompressible (see figure 2). The vein radius undergoing rhythmic, peristaltic contractions is given by $a(z,t)$, where z is the longitudinal coordinate along the vein and t time. The radial coordinate is denoted by r. We consider for simplicity that the vein has cylindrical symmetry. The flow field inside the vein is $v_r(r,z,t)$ in the radial direction and $v_z(r,z,t)$ along the vein axis, while pressure is written as $p(r,z,t)$.

We start by calculating relevant non-dimensional numbers characterizing the flow to simplify the Navier–Stokes equations describing the flow field in the contractile vein.

First, vein contractions can be treated within the lubrication approximation, where the wavelength of the peristaltic contractions λ is larger than the average vein radius a_0. In fact, in *P. polycephalum*, the contractile wavelength typically extends over the organism's size [10], $\lambda \simeq 5$ mm, while the typical radius of a vein is $a_0 \sim 100\ \mu$m. Hence, we can define the small non-dimensional number $\epsilon_\lambda = a_0/\lambda \ll 1$. We can, therefore, apply the lubrication approximation, which will allow us to keep only first-order terms in ϵ_λ in the Navier–Stokes equations using the hierarchy of derivatives $\frac{\partial v_z}{\partial r} \sim \frac{1}{\epsilon_\lambda}\frac{\partial v_r}{\partial r} \sim \frac{1}{\epsilon_\lambda}\frac{\partial v_z}{\partial z} \sim \frac{1}{\epsilon_\lambda^2}\frac{\partial v_r}{\partial z}$, see also e.g. [47, 54, 55].

Second, the appropriate Reynolds number for flows in contractile veins is $\mathrm{Re} = \frac{\rho c a_0}{\mu}\epsilon_\lambda$ [56] where c is the typical speed of the contractile wave, μ is the dynamic viscosity and ρ the fluid density. A typical value for the cytoplasmic viscosity is $\mu = 1.5 \times 10^{-3}$ Pa · s [57, 58]. The speed of the contractile wave is $c = \lambda/T$ where $\lambda \simeq 5$ mm is the scale of the organism and $T \simeq 1$–2 min is the contraction period measured in *P. polycephalum* [10, 34, 35]. We find $c \simeq 50\ \mu\text{m} \cdot \text{s}^{-1}$ also agreeing with flow velocities inside veins, directly

Table 1. List of all assumptions used in the derivation and specificity with respect to *P. polycephalum*.

Assumption	Applicability in *P. polycephalum*	Applicability in other systems
Enclosed fluid		
Low Reynolds numbers	Yes [10, 36]	Also low in leaves [48]; intermediate to high Reynolds in blood flow [49] but low in blood vasomotion [50]
Newtonian fluid/Poiseuille flow	Yes [36, 37]	Works well in leaf venation [48, 51]; Non-newtonian models better describe blood flow [52], and point to a possible extension
No slip at the wall	Yes, but slip could be investigated in line with flow inside the porous shell [32, 53]	Works well in blood flow vasculature [43], in leaves [48]
Incompressible fluid	Yes	Common approximation in blood flow [43] and leaves [48], extensions to compressible wave propagation exist [47]
Lubrication approximation $\partial a/\partial z \ll 1$	Yes	Common approximation [43, 54]
Encapsulating shell		
Viscoelastic solid shell	Yes, but the porosity of the shell could be explored in *P. polycephalum* [32]	Works well in blood flow vasculature [43] or leaf venation [46]
Thickness of the visco-elastic shell $e/a \simeq$ const.	Yes, see figure 4, but could account for thickness dynamics in a more detailed investigation	Common approximation for vasculature models with a thin shell [41–45, 47]
Orthogonal response of the shell when sheared	Yes, since the shell is made mostly of an actomyosin cortex for which this response exists [31]	See section 5.2.
Dynamics		
Presence of short and long timescale variations	Yes, due to actomyosin-powered contractions	These are washed out by visco-elastic features of the shell in any case, which is quite common in models [41–45, 47]

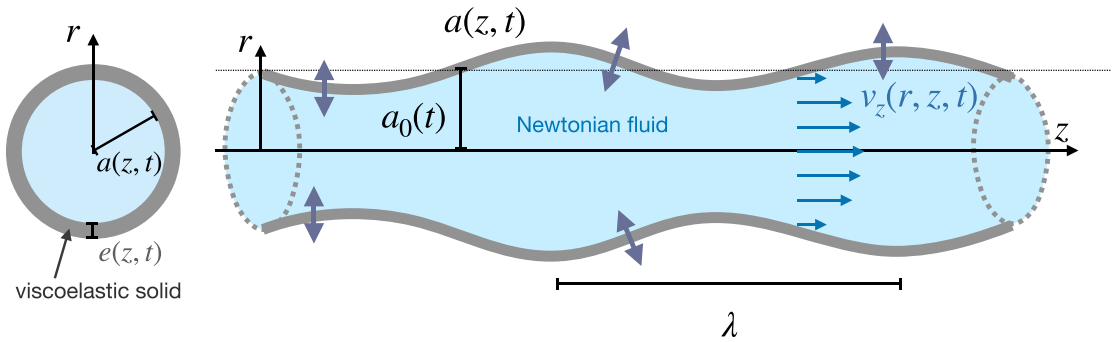

Figure 2. Cross-sectional and longitudinal sketch of a vein of radius $a(z,t)$ filled with fluid flowing with longitudinal speed $v_z(r,z,t)$, where z is the longitudinal coordinate and r the radial one. The vein is encapsulated in a thin viscoelastic shell of thickness $e(z,t)$. Other variables are described in the main text.

measured from our own velocimetry measurements [13]. Taking the density ρ of water, this yields $\mathrm{Re} \simeq 0.003\epsilon_\lambda$ where $\epsilon_\lambda \ll 1$, which enables us to neglect non-linear terms in the Navier–Stokes equations.

Finally, we evaluate the Womersley number $\alpha_W = \sqrt{\frac{\rho a_0^2 \omega}{\mu}}$ [59] with $\omega = 2\pi/T$. The Womersley number quantifies the relative importance of time-dependent inertial terms in the Navier–Stokes equation with respect to viscosity terms. We find $\alpha_W \simeq 0.02$. We can therefore neglect time-dependent inertial terms in the Navier–Stokes equations.

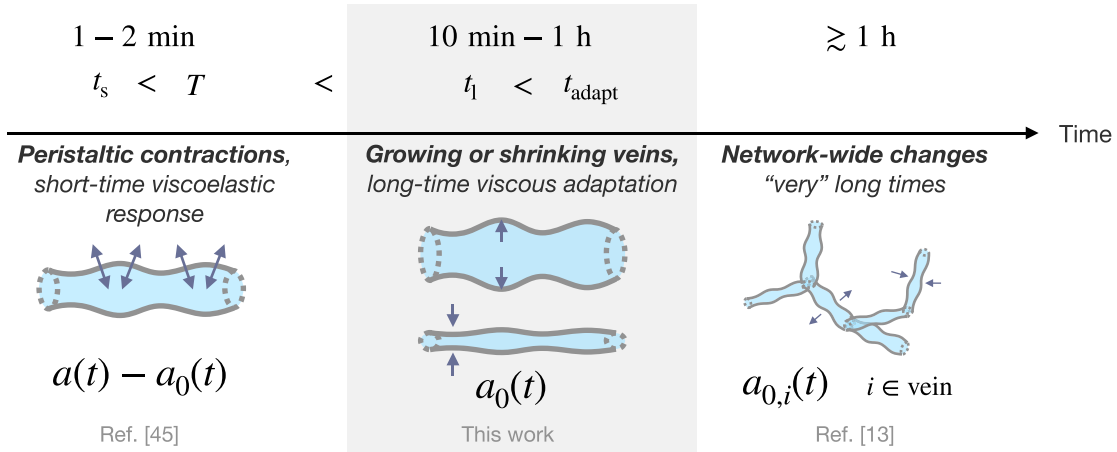

Figure 3. Sketch of the timescales dictating the time evolution of a vein's radius in *P. polycephalum*. Here, we are interested in adaptation at the single vein level, over long timescales corresponding to average growth or shrinkage of the vein.

All in all, the Navier–Stokes equations describing the flow field inside the vein reduce to

$$\begin{cases} 0 = -\dfrac{\partial p}{\partial z} + \mu \dfrac{1}{r}\dfrac{\partial}{\partial r}\left(r\dfrac{\partial v_z}{\partial r}\right), \\ \dfrac{1}{r}\dfrac{\partial (r v_r)}{\partial r} + \dfrac{\partial v_z}{\partial z} = 0. \end{cases} \tag{3}$$

Notice that although we arrived at such equations by determining that the non-dimensional numbers ϵ_λ, Re and α_W are small in *P. polycephalum*, these numbers are usually small across a wide variety of biological systems [54].

Solving these equations in the limit of the lubrication approximation where the dependence of $\frac{\partial p}{\partial z}$ on r can be neglected yields the flow profiles [10]

$$\begin{cases} v_z(r,z,t) = & -\frac{a^2(z,t)}{4\mu}\frac{\partial p}{\partial z}\left(1 - \left(\frac{r}{a(z,t)}\right)^2\right), \\ v_r(r,z,t) = & \frac{\partial a(z,t)}{\partial t}\frac{r}{a(z,t)}\left(2 - \left(\frac{r}{a(z,t)}\right)^2\right) \\ & -\frac{a(z,t)^2}{4\mu}\frac{\partial p}{\partial z}\frac{r}{a(z,t)}\frac{\partial a(z,t)}{\partial z}\left(1 - \left(\frac{r}{a(z,t)}\right)^2\right). \end{cases} \tag{4}$$

Finally, conservation of mass imposes that, along the vein,

$$\frac{\partial}{\partial t}\left(\pi a^2(z,t)\right) = -\frac{\partial}{\partial z}\left(2\pi \int_0^{a(z,t)} v_z(r,z,t)\, r dr\right) = -\frac{\partial}{\partial z}\left(-\frac{\pi a^4}{8\mu}\frac{\partial p}{\partial z}\right) \tag{5}$$

and allows us to infer an equation relating the pressure field p to the contraction profile $a(z,t)$. The remaining missing equation to fully characterize the four variables p, $a(z,t)$, v_r, and v_z corresponds to the force balance on the vein wall, which we detail in section 3.

Finally, longitudinal variations along the vein segment axis z, $\partial a/\partial z \sim \epsilon_\lambda$ can be neglected, as we assumed $\epsilon_\lambda \ll 1$. From now on, we therefore use $a(t) = a(z,t)$.

2.3. Timescales of the vein radius evolution $a(t)$

We will here seek an equation on the evolution in time of the vein radius $a(t)$, via force balance on the vein wall. To understand precisely what this equation will mean, it is relevant to discuss as a preliminary the characteristic time variations of $a(t)$.

The radius of the vein evolves in time according to processes occurring at three different timescales—see figure 3. In order of short to long, (i) peristaltic contractions induce short-time vein deformations; then (ii) veins deform on longer timescales corresponding to growth or disassembly of the wall material; (iii) eventually, network-wide adaptation occurs. Here, we are interested in (ii), which requires to coarse-grain over the short time peristaltic contractions of (i). To distinguish the two timescales (i)–(ii), we will consider the averaging operator $\langle\cdot\rangle$, which is an average over short timescales, typically corresponding to the short peristaltic contractions in *P. polycephalum*. We define this averaging operator precisely in section 3.2.2. The

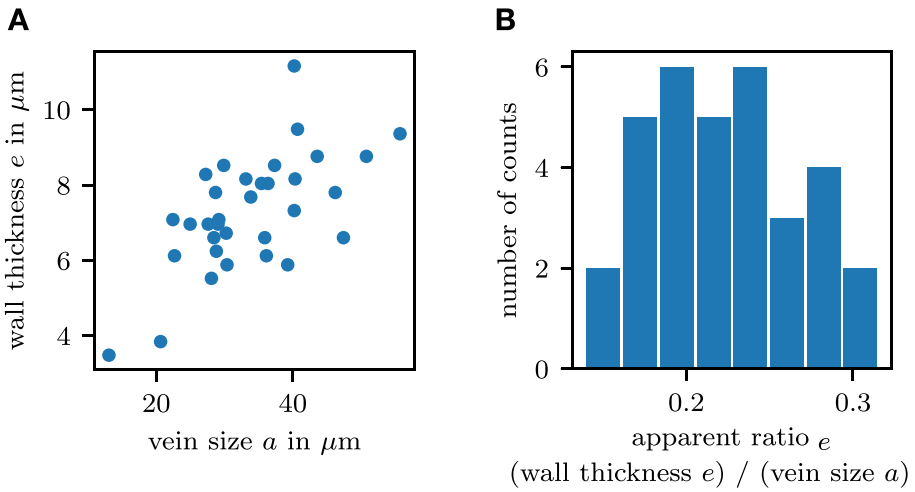

Figure 4. (A) Apparent wall thickness e versus vein size a for 33 randomly selected veins of the specimen in figure 1. The Pearson correlation between e and a is 0.63, and the data is indeed correlated with a p-value $p < 10^{-4}$. (B) Histogram distribution of the associated apparent ratios e/a for all 33 veins.

short-time averaged radius $a_0(t) \equiv \langle a(t) \rangle$ therefore only has variations over long timescales, corresponding to growth or disassembly. In contrast, $a(t) - a_0(t)$ corresponds to short-time peristaltic deformations.

We can neglect inertial relaxation on the vein dynamics. We can demonstrate this by comparing typical timescales. The density of the vein wall is typically $\rho_C \simeq 10^3\ \mathrm{kg\,m^{-3}}$. We seek an upper bound on the relaxation of inertia. Since values for the gel viscosity vary in the literature [39, 40, 45] we use a lower estimate for the gel viscosity $\eta \simeq 240\ \mathrm{Pa \cdot s}$. This implies that the timescale for the relaxation of inertia is at most $t_{\mathrm{inertia}} = \frac{a^2 \rho_C}{\eta} \simeq \frac{10^3 \times (50.10^{-6})^2}{240} \simeq 10^{-8}$ s. Hence, t_{inertia} is much shorter than any other relevant timescale in the system.

2.4. Thickness of the vein walls

We must also discuss how the vein wall's thickness evolves. Direct observations on the specimen presented in figure 1 over several vein sizes suggest the thickness of the vein wall e is correlated with the vein size a (see figure 4). This means the ratio of thickness to size is roughly constant $e/a \simeq \mathrm{const}$. Since different vein sizes represent veins at different adaptation stages, we can assume that in general and with time, this ratio is a constant $\epsilon_e \equiv \langle e(t) \rangle / \langle a(t) \rangle$. The typical ratio we observe from microscopy is $\epsilon_e \simeq 0.1 - 0.3$. Considering the tubular geometry and ensuing variations in light absorption, this ratio could be slightly overestimated.

When veins shrink, they at most shrink down to some small radius value $a \simeq 10$–$20\ \mu$m and then are 'retracted' into the network. Hence, the proportionality relation $e/a = \epsilon_e$ is also satisfied even in small veins, and the thickness of a vein wall never vanishes.

In the following, we will, therefore, consider the thin shell approximation. For simplicity, we will only model the dynamics for $a(t)$, assuming that the dynamics for the vein thickness $e(t)$ closely follow that of the radius $a(t)$.

3. Force balance on a vein wall

3.1. Force balance and viscoelastic response of the tube wall

We will now balance forces on a vein wall for a small, ring-like vein segment of infinitesimal length $\delta\ell$ and radius a. Since we are interested in vein adaptation dynamics, that is to say, in the time evolution of a, we will enumerate all the circumferential stresses, since these are the only ones that may contribute to radius dilatation or shrinkage. The sum of all these stresses results in contributions σ_{tot}. Notice that any radial stress σ_{rr}, such as pressure p, can be positioned in the circumferential direction as $\sigma_{rr} a/e$ where e is the vein thickness and a its radius, within the thin shell approximation [43].

These circumferential stresses σ_{tot} are balanced by tensile and viscous adaptation of the vein wall, for which we establish a minimal model.

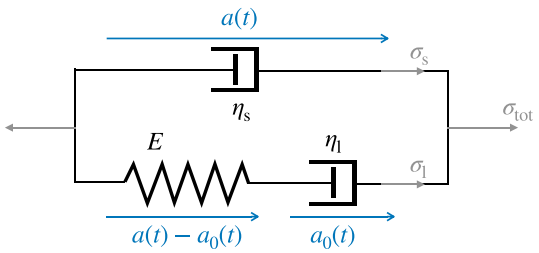

Figure 5. Schematic of the viscoelastic response model of a vein's wall.

3.2. Viscoelastic response of the vein wall

3.2.1. Elastic response

For vein walls such as the ones making up *P. polycephalum*, the Hamiltonian describing the potential energy of the vein wall can assume various forms [45, 60–63], corresponding to various effects such as elasticity, bending, stretching forces, *etc*. Here, we assume linear Hookean-type feedback for elasticity which is a good model for thin elastic shells [43, 47, 64]. Note that the following derivation may be done in a similar way for other Hamiltonians, including *e.g.* bending terms. In practice, in the limit of small deformations, these should yield similar contributions to the response and should not modify the result of this work significantly. With elasticity only, the total external circumferential stresses on the vein wall are balanced by the elastic response

$$\frac{E}{(1-\nu^2)}\frac{(a(t)-a_0(t))}{a_0(t)} = \sigma_{\rm tot} \tag{6}$$

where E is Young's modulus, in Pa, characterizing the wall's elasticity and ν is the material's Poisson's ratio, which is a number with no units [43, 65]. Here we assumed that the reference radius $a_0(t)$ can slowly evolve in time.

3.2.2. Viscoelastic response

Beyond elasticity, the gel-like material making up the tube wall is best described by a viscoelastic solid [39, 40, 45], and we must add the viscous response to equation (6).

3.2.2.1. Short-time viscoelastic response

Previous models on *P. polycephalum* aiming to describe the short-time peristaltic response use the Voigt model for a viscoelastic solid [40, 43, 47] which gives

$$\frac{E}{(1-\nu^2)}\left(\frac{a(t)-a_0}{a_0}+\frac{\eta_{\rm s}}{E}\frac{1}{a_0}\frac{da(t)}{dt}\right) = \sigma_{\rm tot} \tag{7}$$

where η_s is the viscosity of the viscoelastic solid shell, and in these models it is assumed that the reference state a_0 does not evolve, i.e. does not grow or shrink. This model introduces a viscous adaptation time $t_{\rm s} = \eta_{\rm s}/E$ of the material making up the vessel wall, which for *P. polycephalum* can be calculated to be typically $t_{\rm s} \simeq 1$ min [45]. This timescale corresponds to the contraction period T of *P. polycephalum*, and is likely related to actin fiber turnover, happening typically on a 1–2 min timescale (as measured e.g. in HeLa cells [66, 67]).

3.2.2.2. Long-time viscoelastic response

The above model, however, does not reflect long-time adaptation and restructuration of the veins, corresponding e.g. to several rounds of actin fiber turnover, on timescales much longer than 1–2 min.

To model these longer adaptation mechanisms, a potential strategy is to add a viscous behavior in the viscoelastic model as presented in figure 5. Investigating different combinations of viscous/elastic contributions, we have found that adding a Maxwell behavior with another viscosity coefficient η_l — see figure 5 — is the simplest model which reproduces the intrinsic features of our system. To solve for the strain/stress relations in this model, it is useful to introduce $\sigma_{\rm s}$ and $\sigma_{\rm l}$ which represent the stresses distributed on each branch, such that $\sigma_{\rm s}+\sigma_{\rm l}=\sigma_{\rm tot}$, $\sigma_{\rm s}=\eta_{\rm s}da/dt$ and

$$E\frac{a(t)-a_0(t)}{a_0(t)} = \eta_{\rm l}\frac{1}{a_0(t)}\frac{da_0(t)}{dt} = \sigma_{\rm l}. \tag{8}$$

Taking the time derivative of equation (8) recovers a Maxwell law for σ_l along the bottom branch. This introduces a timescale for long-time adaptation $t_\mathrm{l} = \eta_\mathrm{l}/E \gg \eta_\mathrm{s}/E$. We will see in section 4 how to incorporate this latter ingredient in the force balance at long time scales. Before pursuing, it is useful, however, to characterize short-time averages further. The above short-time viscous response equation (7) suggests to define a short-time averaging

$$\langle X(t)\rangle = \frac{1}{t_\mathrm{s}}\int_0^t X(t')\, e^{-\left(t-t'\right)/t_\mathrm{s}}\mathrm{d}t' \tag{9}$$

and we define the short-time averaged vein radius as $a_0(t) \equiv \langle a(t)\rangle$. With this definition, one can investigate long-time adaptation via

$$\left\langle \frac{da(t)}{dt}\right\rangle = \frac{a(t) - a(0)\, e^{-t/t_\mathrm{s}} - a_0(t)}{t_\mathrm{s}} \simeq \frac{a(t) - a_0(t)}{t_\mathrm{s}} \tag{10}$$

where the last equation is obtained by considering we are exploring times $t \gg t_\mathrm{s}$. Using equation (8), we obtain

$$\left\langle \left((a(t) - a_0 + \frac{\eta_\mathrm{s}}{E}\frac{da(t)}{dt}\right)\right\rangle = \frac{\eta_\mathrm{l}}{E}\frac{da_0(t)}{dt}. \tag{11}$$

In general, we expect short timescale variations to be small compared to long timescale variations $|X - \langle X\rangle|/\langle X\rangle \ll 1$. This is especially true in *P. polycephalum* for radius dynamics where radius values oscillate periodically by about 5 μm over short timescales of 1–2 min while vascular adaptation ranges typically up to 50 μm on long timescales of 10–30 min [13]. This means we can approximate, for any variable X and Y, $\langle XY\rangle \simeq \langle X\rangle\langle Y\rangle$, and $\langle 1/X\rangle \simeq 1/\langle X\rangle$. We, therefore, obtain the following simple relation between the short-time response and the long-time response:

$$\left\langle \frac{E}{(1-\nu^2)}\left(\frac{(a(t)-a_0}{a_0} + \frac{\eta_\mathrm{s}}{E}\frac{1}{a_0}\frac{da(t)}{dt}\right)\right\rangle = \frac{\eta_\mathrm{l}}{(1-\nu^2)}\frac{1}{a_0}\frac{da_0(t)}{dt} = \langle\sigma_\mathrm{tot}\rangle\,. \tag{12}$$

3.3. Enumeration of forces

3.3.1. Hydrodynamic forces

Let $\Pi = -p\mathbb{I} + \sigma$ be the tensor characterizing hydrodynamic forces per unit area, where p is pressure, σ is the deviatoric stress tensor and $\mathbb{I}$ is the identity matrix. The hydrodynamic forces acting in the radial direction on the vein's wall are then

$$\delta F_\mathrm{hydro} = (-\delta S\boldsymbol{e_r})\cdot\Pi\cdot\boldsymbol{e_r} + (\delta S\boldsymbol{e_r})\cdot(-p_\mathrm{ext}\mathbb{I})\cdot\boldsymbol{e_r} = \delta S(-\Pi_{rr} - p_\mathrm{ext}) \tag{13}$$

where $\boldsymbol{e_r}$ is the unit vector in the outward radial direction, $\delta S = 2\pi a\delta\ell$ is the infinitesimal surface area of the vein, and p_ext is the atmospheric pressure exerted uniformly across the organism on the outer side of vein walls.

We now calculate the radial components of the tensor $\Pi_{r\ldots}$ to obtain the hydrodynamic forces

$$\begin{cases} \Pi_{rr}|_{r=a} = -p + 2\mu\dfrac{\partial v_r}{\partial r}, \\ \Pi_{rz}|_{r=a} = \mu\left(\dfrac{\partial v_r}{\partial z} + \dfrac{\partial v_z}{\partial r}\right). \end{cases} \tag{14}$$

Note that we also calculate $\Pi_{rz}|_{r=a}$ since we will use it later. Within the lubrication approximation, we have the hierarchy $\frac{\partial v_z}{\partial r} \sim \frac{1}{\epsilon_\lambda}\frac{\partial v_r}{\partial r} \sim \frac{1}{\epsilon_\lambda}\frac{\partial v_z}{\partial z} \sim \frac{1}{\epsilon_\lambda^2}\frac{\partial v_r}{\partial z}$ and further $p \sim \mu\frac{1}{\epsilon_\lambda^2}\frac{\partial v_r}{\partial r}$. Keeping only highest order terms in ϵ_λ yields

$$\begin{cases} \Pi_{rr}|_{r=a} \simeq -p \\ \Pi_{rz}|_{r=a} \simeq \mu\dfrac{\partial v_z}{\partial r}|_{r=a} \end{cases}. \tag{15}$$

Using the expression for the flow profile equation (4) we obtain

$$\frac{\partial v_z}{\partial r} = +\frac{a(z,t)}{2\mu}\frac{\partial p}{\partial z}\frac{r}{a(z,t)} \tag{16}$$

and finally taking its value at the channel boundary we obtain

$$\begin{cases} \Pi_{rr}|_{r=a} \simeq -p \\ \Pi_{rz}|_{r=a} \simeq -\dfrac{4\mu\bar{v}}{a} \end{cases} \tag{17}$$

where $\bar{v}(z,t) = -\frac{a^2(z,t)}{8\mu}\frac{\partial p}{\partial z}$ is the cross-sectional average of v_z. The Π_{rz} component of the stress corresponds to the shear stress, which is related to the shear rate $\tau = \frac{4\bar{v}}{a} = \frac{4Q}{\pi a^3}$ where $Q = \pi a^2 \bar{v}$ via the dynamic viscosity: $|\Pi_{rz}|_{r=a}| = \mu|\tau|$.

Geometrically, only the radial hydrodynamic stresses Π_{rr} can contribute to the circumferential adaptation. We obtain that the resulting hydrodynamic contributions on the vein's wall are simply related to the pressure imbalance, in the circumferential direction

$$\sigma_{\text{hydro}} = \frac{a(t)}{e(t)}(p - p_{\text{ext}}). \tag{18}$$

We note that larger pressure differences between the hydrostatic pressure p and the atmospheric pressure p_{ext} dilate veins as expected. Importantly, we remark that shear stress has no contribution to the radial hydrodynamic stresses.

3.3.2. Active forces

We denote σ_{active} the active stress operated by the actomyosin cortex [40, 68]. We assume these active stresses induce short timescale dynamics that are purely elastic deformations. The short timescale here corresponds to the period of the peristaltic contractions. A chemical potentially triggers these active forces driving contractions within the cytoplasm [40, 45, 63, 68]. Here, we assume that the chemicals are initially well mixed, meaning that the organism has received no localized food or chemical stimulus spatially altering the chemical balance. Throughout the analysis, we further assume that these compounds remain well mixed. This allows us to consider that the active forces do not show any significant trend on long timescales, such that

$$\langle \sigma_{\text{active}} \rangle \simeq \text{const.} \tag{19}$$

where $\langle . \rangle$ denotes the average over short timescales. We will be more specific as to what enters that constant later. We consider that σ_{active} is a radial stress that needs to be multiplied by a factor $a(t)/e(t)$ to enter the circumferential force balance equation (7).

3.3.3. Nonlinear orthogonal feedback forces from shear stress

Shear stress, here denoted as $\Pi_{rz} = \sigma_{rz}$, is considered to be the dominating mechanical force for growth induced by shearing cells in numerous experiments [69, 70]. The importance of shear stress forces for adaptation dynamics could be explained by mechanosensitive pathways [71] or other chemical pathways that regulate the dilatation of veins [72, 73]. However, as we are interested in force balance, we must investigate the contribution of shear stress to forces. Shear stress exerts a force in the *longitudinal* direction on the vein wall—as seen in section 3.3.1—and, hence, can not contribute *a priori* to the radial (or circumferential) forces that dilate or contract the vein.

However, shearing the actomyosin cortex can lead to a significant *orthogonal* response, usually termed *normal* stress, because of the crosslinked structure of the actomyosin gel [30, 31, 74]. We, here, hypothesize (and justify below) that this orthogonal response contributes a circumferential extensional stress $\sigma_{\text{gel}}(\sigma_{rz})$ where $\sigma_{rz} = \Pi_{rz}|_{r=a}$ is the shear stress at the wall and $\sigma_{\text{gel}}(\sigma)$ has units of stress and depends on shear stress at the wall, possibly in a nonlinear way, and its order of magnitude is comparable or greater to that of shear stress [31]. This orthogonal response solves the apparent paradox of how shear stress, via force balance, can act in the radial direction.

3.3.3.1. How can we understand this orthogonal stress?

Janmey *et al* [31] explores the normal stress resulting from shearing a variety of biogels that are crosslinked through semi-flexible or rigid filaments. The gels are sheared between two plates, and experiments identify an orthogonal response with a 'negative' normal stress, meaning that the plates are attracted towards one another—see figure 6(A). This effect is due to the rigid filaments crosslinking the gels that resist shearing by bringing fibers closer to one another, creating the normal stress [30, 31].

3.3.3.2. Could the P. polycephalum cortex also exhibit an orthogonal response?

The negative normal stress is seen across many forms of biogels [74, 75] and is confirmed by minimal numerical models [76] and nonlinear elastic theory [74]. Most experiments on cross-linked filaments exhibit a negative normal stress response, while a few of them yield a positive stress response [31]. For non-active

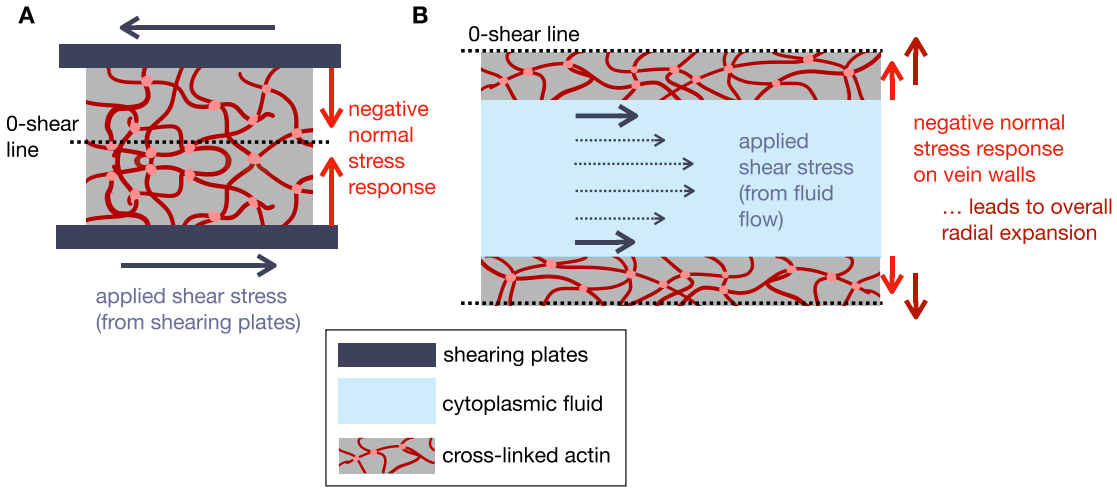

Figure 6. Shear stress leads to radial expansion. (A) Experimental setting of [31] where two plates (dark blue) are shearing a crosslinked gel and a negative normal stress response is observed, that tends to bring the plates together. By symmetry, shear vanishes at the midplane. (B) Analogous effect in a tubular geometry, with a longitudinal view along the vein, where the gel makes up the vein walls. Shear stress from cytoplasmic streaming results in negative compression of the outer actin gel, which, since there is no resistance on the outer wall, leads to an expansion of the vein radius.

interconnected actin filaments the response is indeed negative. References [30, 31] have further identified that the orthogonal negative response is likely due to the material's rigid crosslinks. Crosslinks, including passive crosslinks, are present in the active actomyosin gel; hence, it is a valid assumption that such negative normal stress would be maintained in gels with an active component such as the one making up the outer wall of *P. polycephalum*.

3.3.3.3. How does the orthogonal gel response translate to a vascular geometry?
In our vascular setting with fluid enclosed by an actin cortex gel, the vein wall is sheared between the fluid-gel and the air-gel boundaries; see figure 6(B). Compared to the geometry of the shearing experiments of [31], here, the largest shearing component is located on the inner wall of the vein, such that the negative normal stress should result in compression/thinning of the vein's wall. However, compared to the geometry of the shearing experiments, which includes a 0-shear, 0-motion line, here, there is no resistance on the air-gel side, and the gel can relax stress by expanding on the free-air side. Effectively this means that the inner vein radius increases, with $\sigma_{\rm gel}(\sigma) > 0$. The normal stress increases with increasing shear [31], here resulting in further dilation—consistent with the assumptions of many previous theoretical works [3, 20–23, 25–27]. We hope to motivate further models in the cylindrical geometry to investigate this radial, normal stress response.

3.3.3.4. What happens to the wall thickness?
While one could design a force balance approach accounting for both the relaxation of the inner fluid radius $a(t)$ and the gel thickness $e(t)$, here, we simply assume both evolve in tandem $e \propto a$, as corroborated by experimental data (see figure 4). Again, we hope to motivate further advanced models, which would account for both variations, as well as highly viscous flow within the gel. Note that the vein's fluid and wall mass are not necessarily conserved during the adaptation process, but this is not contradictory. Indeed, fluid mass is brought in and out from other parts of the network, and wall structure is continuously deformed over long timescales, corresponding to *e.g.* several rounds of actin fiber turnover and rearrangements [66, 67].

3.3.3.5. What is the functional dependence of the normal stress on the shear stress?
Nonlinear elasticity theory can predict the normal stress response due to shear stress [74, 76–80]. The magnitude of the normal stress response depends on the mechanical properties of the gel and the crosslinking filaments. Furthermore, the normal response scales linearly or quadratically with the shear rate [74, 76, 79]. Quadratic models accurately reproduce the negative normal stresses observed in [31]. We, therefore, assume in the following that the normal stress can be written

$$\sigma_{\rm gel}(\sigma) = \frac{a(t)}{e(t)}\frac{1}{\sigma_c}\sigma^2, \tag{20}$$

where $\sigma_c > 0$ is a characteristic shear stress quantifying the responsiveness of the gel wall material. Other functional forms, that are monotonically increasing with $\sigma > 0$ and that verify $\sigma_{\rm gel}(\sigma = 0) = 0$, such as

$\sigma_{\rm gel}(\sigma) = |\sigma|$ would not change the main results of this work. Here, only the orthogonal response is essential to derive an adaptation rule from force balance.

3.3.3.6. What timescales are involved in the normal response?
Finally, we need to specify for the orthogonal response what timescales are involved, precisely, whether the shear stress σ_{rz} contributing to the normal response corresponds to short, elastic, or long, viscous, timescale contributions. In *P. polycephalum*, we observe in experiments that vein adaptation, compared to the input shear signal, happens with a time delay [13]. This time delay is typically at least of the order of a contraction period. Hence, the time delay washes out short timescale stress contributions, and only the long timescale dependence of shear is relevant. More generally, we may expect the gel's orthogonal response to occur with a timescale corresponding to actin fiber rearrangements. Therefore the orthogonal response varies only over long timescales. In the following, we prefer to express equations in terms of the shear rate $\tau = \sigma_{rz}/\mu$ such that we may rewrite the radial orthogonal gel response as

$$\sigma_{\rm gel}\left(\mu\langle\tau\rangle\right) = \frac{a(t)}{e(t)}\mu\frac{\langle\tau\rangle^2}{\tau_c}, \tag{21}$$

where we included the fact that the relevant shear is over long timescales. We also define $\tau_c = \sigma_c/\mu$ as the associated characteristic shear rate.

3.4. Force balance on a vein segment

Gathering all stresses as outlined above, we can now write the balance of stresses acting on a vein ring-like section of length $\delta\ell$ as

$$\sigma_{\rm tot} = \frac{E}{(1-\nu^2)}\left(\frac{a(t)-a_0}{a_0} + \frac{\eta_{\rm s}}{E}\frac{1}{a_0}\frac{da(t)}{dt}\right) = \sigma_{\rm hydro} + \frac{a(t)}{e(t)}\sigma_{\rm active} + \sigma_{\rm gel}. \tag{22}$$

Using the expressions derived above for the forces, equations (18) and (21), we obtain

$$\frac{E}{(1-\nu^2)}\left(\frac{a(t)-a_0}{a_0} + \frac{\eta_{\rm s}}{E}\frac{1}{a_0}\frac{da(t)}{dt}\right) = \frac{a(t)}{e(t)}\left(p-p_{\rm ext}\right) + \frac{a(t)}{e(t)}\sigma_{\rm active} + \frac{a(t)}{e(t)}\mu\frac{\langle\tau\rangle^2}{\tau_c}. \tag{23}$$

Note that we neglected any fluctuating forces in this simple force balance, especially as they would eventually be averaged out in the long timescale we focus on here. In addition, we still have the long-time response dictated through equation (8).

4. Long time adaptation model

We now aim to simplify the force balance equation (23). To do so, we use our timescale separation assumption: some variables demonstrate either long timescale dynamics or short timescale dynamics in line with radius dynamics that have both short and long timescales. Long timescale dependencies will, from here on, be written as $\langle X\rangle(t)$ for any variable X.

4.1. Short timescales

We first focus on short timescales. To observe short timescale dynamics, we can take the short-time average of equation (23), use the long-time response of the system equation (12), and subtract it back from equation (23). Reordering terms we obtain an equation characterizing short-timescale dynamics

$$\begin{aligned}\frac{d\left(a(t)-a_0(t)\right)}{dt} = a_0(t)\frac{1-\nu^2}{\eta}\frac{a(t)}{e(t)}\left(\left(p-p_{\rm ext}\right) - \frac{E}{1-\nu^2}\frac{\left(a-a_0(t)\right)}{a_0(t)}\frac{e(t)}{a(t)} + \sigma_{\rm active} + \mu\frac{\langle\tau\rangle^2}{\tau_c}\right)\\ - \left\langle a_0(t)\frac{1-\nu^2}{\eta_{\rm l}}\frac{a(t)}{e(t)}\left(\left(p-p_{\rm ext}\right) + \sigma_{\rm active} + \mu\frac{\langle\tau\rangle^2}{\tau_c}\right)\right\rangle.\end{aligned} \tag{24}$$

In a single tube without peristaltic pumping, $a(t) \simeq a_0(t)$ and equation (24) allows us to characterize the pressure in the system. For example, this would be a necessary equation to completely solve the fluid flow problem since we have *a priori* four unknowns, v_r, v_z, p, and a, and the Navier–Stokes equations only give three equations. Equation (24) relating pressure to circumferential stress and active stresses (or variants) has been used by several authors [45, 63, 81–85] (for example see equation (1*c*) of [82] or equation (3) in [81]). Equation (24) together with the hydrodynamic equations (4) and (5), now form a complete set of equations to calculate flows and contractions at *short* timescales. Our interest goes beyond, to the long timescales, where significant vein adaptation happens.

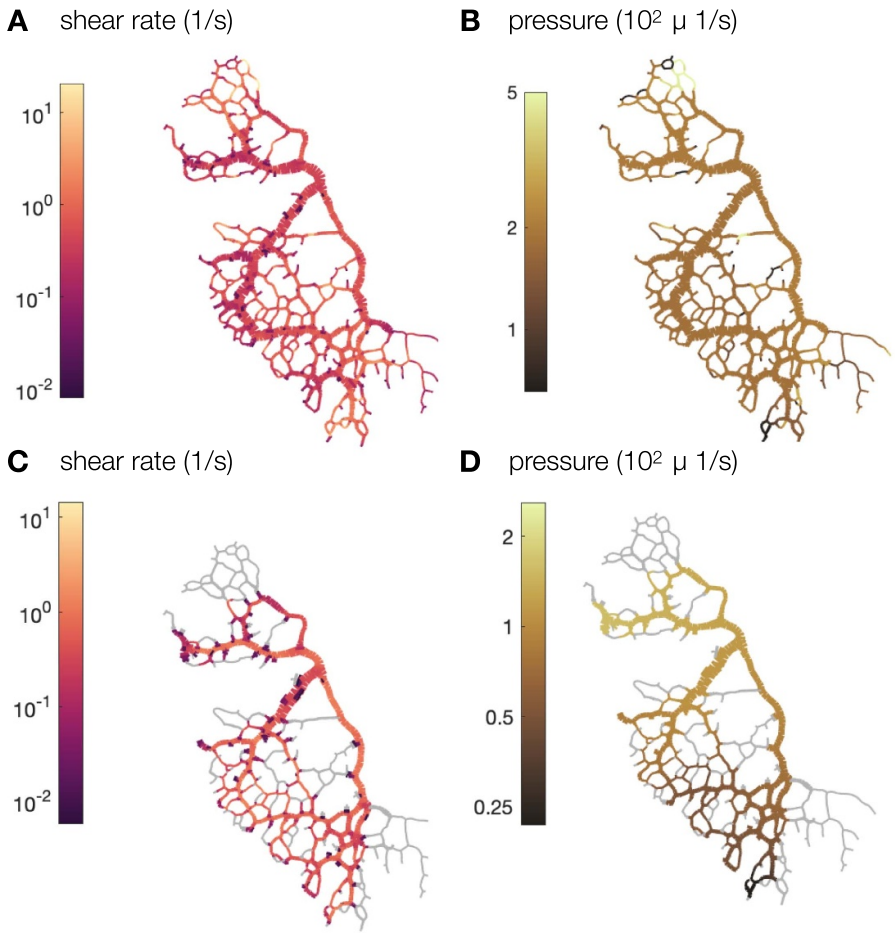

Figure 7. Averaged shear rate (A)–(C) and pressure (B)–(D) in a specimen corresponding to the full network presented in figure 1. The fields are calculated using data from image analysis that provides vein contractions, as well as conservation of mass and Kirchhoff's laws. The results are presented at the initial stage (A)–(B) and the final stage of the experiment, 54 min later (C)–(D). In the final stage, veins that have vanished are represented in gray. More details on calculation methods may be found in [13]. Images are adapted with permission from [13].

4.2. Long timescales

Let us now return to the full force balance equation (23) and average dynamics over the short timescales, use equation (12), to obtain long timescale adaptation,

$$\frac{da_0(t)}{dt} = a_0(t)\frac{1-\nu^2}{\eta}\frac{a_0(t)}{\langle e(t)\rangle}\left(\langle (p-p_{\text{ext}})+\sigma_{\text{active}}\rangle + \mu\frac{\langle\tau\rangle^2}{\tau_c}\right). \tag{25}$$

We now seek possible simplifications on the right-hand side of equation (25).

Firstly, we can consider that $\langle (p-p_{\text{ext}})\rangle$ changes only marginally over long times. Generally, we expect that local pressure can not vary too much at the risk of damaging tissue. In *P. polycephalum* we can verify this assumption by observing calculated pressure fields. In figures 7(B) and (D), we present numerically calculated pressure fields in each vein from network-wide vein contraction data for the specimen shown in figure 1, at the beginning of the experiment and after a significant adaptation time. The details of how the pressure field is calculated are reported in [13]. We find that the pressure field evolves only over less than an order of magnitude over the entire duration of the experiment of an hour. In comparison, shear can vary over three orders of magnitude in the same time frame; see figures 7(A) and (C). Our maps also show that the pressure p is relatively uniform across the network and does not depend on the radius $\langle a\rangle$ of a vein, unlike shear rate. We can therefore consider that $\langle (p-p_{\text{ext}})\rangle$ smoothly evolves across the network and only changes over 'very' long timescales, when significant adaptation happens for many veins in the network—see the right-most panel of figure 3.

Secondly, as we mentioned earlier, $\langle\sigma_{\text{active}}\rangle$ is a constant stress related to the active consumption of energy for wall contractility. Typically, as this stress characterizes the force per unit wall area necessary for contraction, we do not expect it to depend on $\langle a\rangle$. Importantly though, this active stress is related to energy

consumption and hence constantly opposes vein growth; mathematically $\langle \sigma_{\text{active}} \rangle < 0$, it can be thought of as the force analog of the metabolic cost energy $\pi\, bLa^2$ in Murray's derivation in equation (1), see the introduction. We, therefore, expect this component to determine the global sign of $\langle (p - p_{\text{ext}}) + \sigma_{\text{active}} \rangle$ such that we can write $\langle (p - p_{\text{ext}}) + \sigma_{\text{active}} \rangle = -\mu \tau_{\text{target}}$ where $\tau_{\text{target}} > 0$ is a typical target shear rate, characterizing energy consumption, corrected by hydrostatic pressure, that can smoothly evolve across the network and over long timescales, longer than the timescale for local vascular adaptation. Under these conditions equation (25) simplifies to

$$\frac{da_0(t)}{dt} = a_0(t)\,\frac{1-\nu^2}{\eta_{\text{l}}}\,\frac{1}{\epsilon_e}\left(\mu\frac{\langle\tau\rangle^2}{\tau_c} - \mu\tau_{\text{target}}\right), \tag{26}$$

To further simplify this expression, we now introduce the local target shear rate $\tau_0 = \sqrt{\tau_c \tau_{\text{target}}}$ and

$$t_{\text{adapt}} = \frac{1}{1-\nu^2}\,\epsilon_e\,\frac{\eta_{\text{l}}}{\mu\tau_{\text{target}}} \tag{27}$$

as characteristic adaptation timescale for vascular rearrangement.

We, thus, rewrite equation (26) in a more compact way and obtain the adaptation rule

$$\frac{da_0(t)}{dt} = \frac{a_0(t)}{t_{\text{adapt}}}\left(\frac{\langle\tau\rangle^2}{\tau_0^2} - 1\right) \tag{28}$$

as the main result of this work. Note, equation (28) resembles previous phenomenological approaches [3, 8, 18, 20–27] yet, here, arises from force balance on the vein wall.

It is relevant to close our analysis and determine whether the adaptation timescale t_{adapt} gives the correct adaptation timescale in orders of magnitude. For an order of magnitude estimation, we can neglect Poisson's ratio ν; we assume $\mu\tau_{\text{target}}$ is comparable to pressure differences across the organism $\mu\tau_{\text{target}} \simeq 10^2\mu\ 1/\text{s} \simeq 10^{-1}$ Pa. The long time viscous adaptation $\eta_{\text{l}} \simeq 10 - 100\ \eta_{\text{s}} \simeq 10^3 - 10^4$ Pa $\cdot$ s Using in addition $\epsilon_e \simeq 0.1$, we obtain $t_{\text{adapt}} \simeq 10^3 - 10^4$ s. This corresponds indeed to the order of magnitude found from fits of equation (28) to adaptation data in [86].

5. Discussion

In this work, we have established a physical derivation based on force balance to justify the broadly used adaptation rule

$$\frac{1}{a_0}\frac{da_0}{dt} = \frac{1}{t_{\text{adapt}}}\left(f(\tau) - f(\tau_0)\right). \tag{29}$$

For our case study in *P. polycephalum*, where fluid flow is encapsulated by crosslinked fibers making up a gel, we have provided reasoning to support that $f(\tau) = \langle\tau\rangle^2/\tau_0^2$, and this scaling is in agreement with experimental data [31]. We recall that a is the radius of a vein, t time, t_{adapt} a timescale characterizing adaptation, τ shear rate, and τ_0 a steady state shear rate. The notation $\langle . \rangle$ averages out short timescale, elastic deformations, such that the law in equation (29) characterizes long timescale deformations.

Our force-balance approach is based on fluid flow physics and on the detailed enumeration and investigation of forces at play on the vessel wall, namely: hydrodynamic forces that are pressure and normal stress, conservative forces such as circumferential stress, active stresses, orthogonal feedback from shear stress, and friction forces. We have proposed a potential mechanism where over long timescales corresponding to viscous deformations, the dominant forces are orthogonal feedback forces from shear stress. These are due to a unique feature of crosslinked fiber networks making up the actomyosin cortex. When the fibers are sheared, the crosslinks between them bring them closer together, resulting in a normal response under shear. This response tends to dilate vessels when the shear rate increases.

We now discuss our model's validity relative to other works and other systems beyond *P. polycephalum*, specific insight on equation (29), and possible extensions.

5.1. Validity of the derivation with respect to existing theories

The result in equation (28) has the same mathematical shape as the phenomenological equation (2) used in many prior works [3, 8, 18, 20–27]. It is therefore consistent with these phenomenological laws while bringing physical validation and insight. Our result is also consistent with Murray's steady state assumption. In fact, the steady state of equation (28) corresponds to a constant average shear rate in the vein $\langle\tau\rangle = \tau_0$. Compared to existing theories where short timescale elastic deformation of veins is not discussed, here we

provide a distinction between viscous and elastic deformations, and our adaptation rule corresponds to viscous, long time, deformations. The relevant or sensed shear rate for adaptation feedback is the long timescale one, $\langle\tau\rangle$, where short-lived elastic contributions are averaged out.

5.2. Applicability of the derivation in other vasculature systems

While our derivation is set in the context of *P. polycephalum*, most of the assumptions we make are standard in vasculature studies [41–45, 48], as we also recapitulate in table 1. The main original assumption is the feedback mechanism for shear on adaptation, originating from the orthogonal response of the cross-linked gel, discussed in section 3.3.3. Such an orthogonal response is quite likely in many soft bio-gels [30, 31] and therefore quite likely to occur in different settings. For endothelial cells lining animal vasculature the cell reorientation upon shear along the tube thereby thinining tube diameter might similarly result in an orthogonal response [87].

5.3. Functional dependence of the feedback on shear rate τ

In our derivation, we obtain that the adaptation function is quadratic, $f(\tau) = \frac{\langle\tau\rangle^2}{\tau_0^2}$. This is similar to the functional form used in [3], where the quadratic dependence was obtained phenomenologically from Murray's law. However, the origin of the quadratic dependence lies in the detailed characteristics of the orthogonal response of the gel, namely $f(\tau) \sim \sigma_{\rm gel}(\mu\langle\tau\rangle)$. Hence, different mechanical properties of the gel making up a vein wall could yield different functional forms [76]. Again, we argue that here it is not so much the exact functional dependence that is critical to obtain an adaptation model in the form of equation (2). Rather, the fact that the gel making up the wall exhibits an orthogonal response is key in the force balance approach to obtain radius adaptation from variable shear rate. As mentioned in the text, such orthogonal feedback can be studied more rigorously with nonlinear elastic theories or numerics [74, 76], and we hope to motivate further work in cylindrical geometry.

5.4. New insights from the force balance perspective

The advantage of the force balance approach is that we can now give further physical meaning to the quantities $t_{\rm adapt}$ and τ_0 in the adaptation law equation (2).

The constant $\tau_0 \sim -\langle\sigma_{\rm active}\rangle/\mu - \langle(p - p_{\rm ext})\rangle/\mu$ corresponds to the steady state shear rate in Murray's law. It can, thus, be related to the typical local energy expense to sustain a vein $\sqrt{b/\mu}$, where we recall that b is a local metabolic constant per unit volume and μ fluid viscosity. This contribution corresponds in our derivation to the active stress required to sustain peristaltic contractions $-\langle\sigma_{\rm active}\rangle/\mu \sim \sqrt{b/\mu}$. Here, we bring further insight complementing Murray's derivation, as our adaptation dynamics equation (25) hints that τ_0, or the metabolic cost, also depends on local pressure ($\langle p - p_{\rm ext}\rangle$). Hence, the local target shear rate τ_0 is not just an intrinsic property of the system. Instead, it characterizes minimal energy expense at a given point in the network and smoothly and slowly varies across the network. Interestingly, our approach allows us to integrate the role of hydrostatic pressure in adaptation: when pressure is higher, the constant τ_0 is decreased, favoring veins with *ab initio* lower shear rate $\langle\tau\rangle$ to grow, in line with the physical intuition that high hydrostatic pressures may drive vein dilation.

We can also draw insight on the adaptation timescale $t_{\rm adapt} \sim \eta_l/\mu\tau_0$ as it includes the parameters of the model. If the local target shear rate τ_0 is small, corresponding to a lower energy consumption level or larger local pressure that helps to keep the vein open, then $t_{\rm adapt}$ is long, and the vein is not prone to fast vascular adaptation. Reversely, if τ_0 is large, vein adaptation can happen fast. Furthermore, the adaptation is slow coherently if the resistance to viscous change η_l is large.

Finally, it is important to note that $t_{\rm adapt}$ and τ_0 form two independent parameters characterizing the adaptation dynamics in equation (28), and that both vary smoothly across the network. In fact, the parameters that define $t_{\rm adapt}$ and τ_0, namely η_l, μ, and τ_c depend on mechanical and fluidic properties that vary across an individual organism as a function of both vein maturation and size [39, 57, 58, 88] as well as integrated exposure to light [89]. The parameters η_l, μ and τ_c also vary among different specimens due to the responsiveness to ambient conditions, such as humidity [90, 91], light conditions [90, 92–94] and temperature [95, 96]. For example, the cytoplasm viscosity μ can vary depending on the local content of salt concentration or dispersed particles inside veins [58]. Furthermore, both η_l and τ_c are related to the cortex mechanical properties, whose structure varies both within a specimen and over time [39, 88].

5.5. Comments on extensions of the model and conclusion

In our adaptation model, we consider a section of the vein that communicates only via flow with the rest of the network. A more detailed model could describe, for example, the dynamics of the retraction phase of a vein from its dangling end. As these are typically short events, achieved within less than a contraction period, compared to vein dynamics such as shrinking or growing that can extend over several contraction periods,

we chose to ignore them in our long timescale adaptation model. Finally, other feedback mechanisms could be explored in more detail, such as fiber resistance to deformation [97], wall thickness adaptation [26], including the porosity of the wall [32] and testing the impact of poro-elasticity [98], or finally in time including energy or oxygen transport [27].

In conclusion, the model derived from force balance incorporates as few assumptions as possible to arrive at the adaptation rule equation (2). Using the quadratic dependence of the adaptation function $f(\tau) = \langle\tau\rangle^2/\tau_0^2$, we have shown in our accompanying work [13], that even these simple assumptions are sufficient to reproduce a variety of adaptation dynamics that are observed experimentally. Furthermore, although our force balance derivation and subsequent experimental investigation were adapted to the model organism *P. polycephalum*, the underlying physical principles of fluid flow physics and mechanical response are universal. Hence, we believe adaptation models based on force balance approaches are relevant to study vascular adaptation across further flow networks in plants and animals.

Data availability statement

All data that support the findings of this study are included within the article.

Acknowledgments

The authors are indebted to Charles Puelz for enlightening discussions on force balance in veins and Emilie Verneuil and Nicolas Bain for discussions on the orthogonal response of sheared gels. They would also like to thank Leonie Bastin and Felix Bäuerle for interesting discussions on *P. polycephalum*. S M was supported in part by the MRSEC Program of the National Science Foundation under Award Number DMR-1420073. This work was supported by the Max Planck Society and has received funding from the European Research Council (ERC) under the European Union's Horizon 2020 research and innovation program (Grant Agreement No. 947630, FlowMem).

ORCID iDs

Sophie Marbach https://orcid.org/0000-0002-2427-2065
Karen Alim https://orcid.org/0000-0002-2527-5831

References

[1] Lucitti J L, Jones E A V, Huang C, Chen J, Fraser S E and Dickinson M E 2007 *Development* **134** 3317–26
[2] Chen Q, Jiang L, Li C, Hu D, Bu J-W, Cai D, Du J-L and Krasnow M 2012 *PLoS Biol.* **10** e1001374
[3] Hu D and Cai D 2013 *Phys. Rev. Lett.* **111** 138701
[4] Kurz H 2000 *J. Neuro-Oncol.* **50** 17–35
[5] Hove J R, Köster R W, Forouhar A S, Acevedo-Bolton G, Fraser S E and Gharib M 2003 *Nature* **421** 172–7
[6] Zhou Y, Kassab G S and Molloi S 1999 *Phys. Med. Biol.* **44** 2929
[7] Corson F, Adda-Bedia M and Boudaoud A 2009 *J. Theor. Biol.* **259** 440–8
[8] Ronellenfitsch H and Katifori E 2016 *Phys. Rev. Lett.* **117** 138301
[9] Tero A, Takagi S, Saigusa T, Ito K, Bebber D P, Fricker M D, Yumiki K, Kobayashi R and Nakagaki T 2010 *Science* **327** 439–42
[10] Alim K, Amselem G, Peaudecerf F, Brenner M P and Pringle A 2013 *Proc. Natl Acad. Sci.* **110** 13306–11
[11] Meyer E P, Ulmann-Schuler A, Staufenbiel M and Krucker T 2008 *Proc. Natl Acad. Sci. USA* **105** 3587–92
[12] Pries A R, Cornelissen A J M, Sloot A A, Hinkeldey M, Dreher M R, Höpfner M, Dewhirst M W, Secomb T W and Papin J A 2009 *PLoS Comput. Biol.* **5** e1000394
[13] Marbach S, Ziethen N, Bastin L, Bäuerle F K and Alim K 2023 *eLife* **12** e78100
[14] Murray C D 1926 *Proc. Natl Acad. Sci. USA* **12** 207
[15] Kassab G S 2006 *Am. J. Physiol. Heart Circ. Physiol.* **290** H894–903
[16] West G B, Brown J H and Enquist B J 1997 *Science* **276** 122–6
[17] McCulloh K A, Sperry J S and Adler F R 2003 *Nature* **421** 939–42
[18] Akita D, Kunita I, Fricker M D, Kuroda S, Sato K and Nakagaki T 2016 *J. Phys. D: Appl. Phys.* **50** 024001
[19] Fricker M D, Akita D, Heaton L L, Jones N, Obara B and Nakagaki T 2017 *J. Phys. D: Appl. Phys.* **50** 254005
[20] Tero A, Kobayashi R and Nakagaki T 2007 *J. Theor. Biol.* **244** 553–64
[21] Taber L A 1998 *J. Biomech. Eng.* **120** 348–54
[22] Hacking W, VanBavel E and Spaan J 1996 *Am. J. Physiol. Heart Circ. Physiol.* **270** H364–75
[23] Hu D, Cai D and Rangan A V 2012 *PLoS One* **7** e45444
[24] Baumgarten W and Hauser M J B 2013 *Phys. Biol.* **10** 026003
[25] Pries A, Secomb T and Gaehtgens P 1998 *Am. J. Physiol. Heart Circ. Physiol.* **275** H349–60
[26] Pries A R, Reglin B and Secomb T W 2005 *Hypertension* **46** 725–31
[27] Secomb T W, Alberding J P, Hsu R, Dewhirst M W and Pries A R 2013 *PLoS Comput. Biol.* **9** e1002983
[28] Bonifaci V 2017 *J. Math. Biol.* **74** 567–81

[29] Bonifaci V, Mehlhorn K and Varma G 2012 *J. Theor. Biol.* **309** 121–33
[30] Gardel M L, Kasza K E, Brangwynne C P, Liu J and Weitz D A 2008 Mechanical response of cytoskeletal networks *Methods in Cell Biology* vol 89 (Elsevier) ch 19, pp 487–519
[31] Janmey P A, McCormick M E, Rammensee S, Leight J L, Georges P C and MacKintosh F C 2007 *Nat. Mater.* **6** 48–51
[32] Wohlfarth-Bottermann K 1974 *J. Cell Sci.* **16** 23–37
[33] Kamiya N 1981 *Annu. Rev. Plant Physiol.* **32** 205–36
[34] Stewart P A and Stewart B T 1959 *Exp. Cell Res.* **17** 44–58
[35] Isenberg G and Wohlfarth-Bottermann K 1976 *Cell Tissue Res.* **173** 495–528
[36] Kamiya N 1950 *Cytologia* **15** 183–93
[37] Bykov A V, Priezzhev A V, Lauri J and Myllylä R 2009 Doppler OCT imaging of cytoplasm shuttle flow in *Physarum polycephalum J. Biophoton.* **2** 540–7
[38] Alim K 2018 *Phil. Trans. R. Soc.* B **373** 20170112
[39] Fessel A, Oettmeier C, Wechsler K and Döbereiner H-G 2017 *J. Phys. D: Appl. Phys.* **51** 024005
[40] Alonso S, Radszuweit M, Engel H and Bär M 2017 *J. Phys. D: Appl. Phys.* **50** 434004
[41] Bertaglia G, Caleffi V and Valiani A 2020 *Comput. Methods Appl. Mech. Eng.* **360** 112772
[42] Mitsotakis D, Dutykh D, Li Q and Peach E 2019 *Wave Motion* **90** 139–51
[43] Bessems D, Giannopapa C G, Rutten M C M and van de Vosse F N 2008 *J. Biomech.* **41** 284–91
[44] Valdez-Jasso D, Haider M A, Banks H, Santana D B, Germán Y Z, Armentano R L and Olufsen M S 2008 *IEEE Trans. Biomed. Eng.* **56** 210–9
[45] Julien J-D and Alim K 2018 *Proc. Natl Acad. Sci.* **115** 10612–7
[46] Bar-Sinai Y, Julien J-D, Sharon E, Armon S, Nakayama N, Adda-Bedia M, Boudaoud A and Prusinkiewicz P 2016 *PLoS Comput. Biol.* **12** e1004819
[47] Anand V and Christov I C 2020 *Phys. Fluids* **32** 112014
[48] Jensen K H, Berg-Sørensen K, Bruus H, Holbrook N M, Liesche J, Schulz A, Zwieniecki M A and Bohr T 2016 *Rev. Mod. Phys.* **88** 035007
[49] Ku D N 1997 *Annu. Rev. Fluid Mech.* **29** 399–434
[50] Fasano A, Farina A and Caggiati A 2017 *Rev. Vascular Med.* **8** 1–4
[51] Sack L and Holbrook N M 2006 *Annu. Rev. Plant Biol.* **57** 361–81
[52] Sankar D, Jaafar N A and Yatim Y 2016 *Glob. J. Pure Appl. Math.* **12** 1337 (available at: www.google.com/url?sa=t&rct=j&q=&esrc=s&source=web&cd=&ved=2ahUKEwie8-eUj6GDAxUdQaQEHfrcBqIQFnoECA8QAQ&url=https%3A%2F%2Fwww.ripublication.com%2Fgjpam16%2Fgjpamv12n2_15.pdf&usg=AOvVaw1onG3LTr8iqum32BrsOxi1&opi=89978449)
[53] Feng J J and Young Y-N 2020 *Phys. Rev. Fluids* **5** 124304
[54] Marbach S, Dean D S and Bocquet L 2018 *Nat. Phys.* **14** 1108–13
[55] Grün G, Mecke K and Rauscher M 2006 *J. Stat. Phys.* **122** 1261–91
[56] Li M and Brasseur J G 1993 *J. Fluid Mech.* **248** 129–51
[57] Swaminathan R, Hoang C P and Verkman A 1997 *Biophys. J.* **72** 1900–7
[58] Puchkov E 2013 *Biochem. (Mosc.) Suppl. A: Membr. Cell Biol.* **7** 270–9
[59] Womersley J R 1955 *London, Edinburgh Dublin Phil. Mag. J. Sci.* **46** 199–221
[60] Olufsen M S 1999 *Am. J. Physiol. Heart Circ. Physiol.* **276** H257–68
[61] Storm C, Pastore J J, MacKintosh F C, Lubensky T C and Janmey P A 2005 *Nature* **435** 191–4
[62] Barthes-Biesel D 2016 *Annu. Rev. Fluid Mech.* **48** 25–52
[63] Alim K, Andrew N, Pringle A and Brenner M P 2017 *Proc. Natl Acad. Sci.* **114** 5136–41
[64] Kraus H 1967 *Thin Elastic Shells: An Introduction to the Theoretical Foundations and the Analysis of Their Static and Dynamic Behavior* (Wiley)
[65] Takagi D and Balmforth N 2011 *J. Fluid Mech.* **672** 196–218
[66] Salbreux G, Charras G and Paluch E 2012 *Trends Cell Biol.* **22** 536–45
[67] Fischer-Friedrich E, Toyoda Y, Cattin C J, Müller D J, Hyman A A and Jülicher F 2016 *Biophys. J.* **111** 589–600
[68] Radszuweit M, Alonso S, Engel H and Bär M 2013 *Phys. Rev. Lett.* **110** 138102
[69] Hoefer I E, den Adel B and Daemen M J 2013 *Cardiovascular Res.* **99** 276–83
[70] Koller A, Sun D and Kaley G 1993 *Circ. Res.* **72** 1276–84
[71] Fernandes D C, Araujo T L, Laurindo F R and Tanaka L Y 2018 Hemodynamic forces in the endothelium: from mechanotransduction to implications on development of atherosclerosis *Endothelium and Cardiovascular Diseases* (Elsevier) pp 85–95
[72] Lu D and Kassab G S 2011 *J. R. Soc. Interface* **8** 1379–85
[73] Godbole A S, Lu X, Guo X and Kassab G S 2009 *Am. J. Physiol. Heart Circ. Physiol.* **296** H152–8
[74] Vahabi M, Vos B E, De Cagny H C G, Bonn D, Koenderink G H and MacKintosh F 2018 *Phys. Rev.* E **97** 032418
[75] Kang H, Wen Q, Janmey P A, Tang J X, Conti E and MacKintosh F C 2009 *J. Phys. Chem.* B **113** 3799–805
[76] Conti E and MacKintosh F C 2009 *Phys. Rev. Lett.* **102** 088102
[77] Horgan C O and Murphy J G 2011 *J. Elast.* **104** 343–55
[78] Unterberger M J, Schmoller K M, Bausch A R and Holzapfel G A 2013 *J. Mech. Behav. Biomed. Mater.* **22** 95–114
[79] Holzapfel G A, Unterberger M J and Ogden R W 2014 *J. Mech. Behav. Biomed. Mater.* **38** 78–90
[80] Horgan C and Murphy J 2017 *Soft Matter* **13** 4916–23
[81] Shapiro A H 1977 *J. Biomech. Eng.* **99** 126–47
[82] Grotberg J B and Jensen O E 2004 *Annu. Rev. Fluid Mech.* **36** 121–47
[83] Mikelić A, Guidoboni G and Čanić S 2007 *Netw. Heterog. Media* **2** 397
[84] Elbaz S B and Gat A D 2016 *J. Fluid Mech.* **806** 580–602
[85] Acosta S, Puelz C, Rivière B, Penny D J, Brady K M and Rusin C G 2017 *Biomech. Model. Mechanobiol.* **16** 2093–112
[86] Marbach S, Alim K, Andrew N, Pringle A and Brenner M P 2016 *Phys. Rev. Lett.* **117** 178103
[87] Vion A-C, Perovic T, Petit C, Hollfinger I, Bartels-Klein E, Frampton E, Gordon E, Claesson-Welsh L and Gerhardt H 2021 *Front. Physiol.* **11** 623769
[88] Lewis O L, Zhang S, Guy R D and Álamo J C D 2015 *J. R. Soc. Interface* **12** 20141359
[89] Bäuerle F K 2019 On mass transport in Physarum polycephalum (Georg-August Universität)

[90] Rakoczy L 1973 *Ber. Dtsch. Bot. Ges.* **86** 141–64
[91] Takahashi K, Takamatsu A, Hu Z S and Tsuchiya Y 1997 *Protoplasma* **197** 132–5
[92] Hato M, Ueda T, Kurihara K and Kobatake Y 1976 *Cell Struct. Funct.* **1** 269–78
[93] Nakagaki T, Umemura S, Kakiuchi Y and Ueda T 1996 *Photochem. Photobiol.* **64** 859–62
[94] Rodiek B and Hauser M 2015 *Eur. Phys. J. Spec. Top.* **224** 1199–214
[95] Wohlfarth-Bottermann K 1977 *J. Exp. Biol.* **67** 49–59
[96] Hejnowicz Z and Wohlfarth-Bottermann K 1980 *Planta* **150** 144–52
[97] Taber L A 1998 *Biophys. J.* **74** 109–14
[98] Xu Q, Wilen L A, Jensen K E, Style R W and Dufresne E R 2020 *Phys. Rev. Lett.* **125** 238002